Why Au and Cu are more selective than Pt for preferential oxidation of CO at low temperature

S. Kandoi, A.A. Gokhale, L.C. Grabow, J.A. Dumesic, and M. Mavrikakis*

Department of Chemical and Biological Engineering, University of Wisconsin-Madison, Madison, WI 53706, USA

Received 27 October 2003; accepted 12 November 2003

Self-consistent, periodic density functional theory (DFT) calculations and micro-kinetic modeling are used to compare selectivity for the preferential oxidation of CO (PROX) with respect to H_2 based on studies of elementary reaction steps on the (111) facet of Au, Cu and Pt. The first step of H oxidation (OH formation) has a higher activation barrier than the second step (H_2O formation) on all three metal surfaces, indicating that OH formation competes with CO oxidation for the removal of trace amounts of CO from a typical reformate gas. The activation energy barrier for CO oxidation is found to be 0.18 eV on Au(111), 0.82 eV on Cu(111) and 0.96 eV on Pt(111), whereas the barrier for OH formation is 0.90, 1.28 and 0.83 eV respectively. A micro-kinetic model based on the DFT results shows that trends in the selectivity of these metals at different temperatures is due to (i) differences in the rate constants of the competitive CO and H oxidation reactions, and (ii) differences in the CO and H surface coverages. Our results explain why Au and Cu are more selective PROX catalysts compared to Pt at low temperatures. At higher temperatures, Pt and Cu lose some of their selectivity to CO oxidation, whereas the selectivity on Au decreases substantially primarily because of the significantly weaker CO adsorption.

KEY WORDS: density functional theory; fuel cells; catalyst; gold; platinum; copper; preferential oxidation; CO oxidation; hydrogen oxidation; selectivity; micro-kinetic model.

1. Introduction

In recent years, proton exchange membrane (PEM) H_2 fuel cells have been used for power generation in a variety of applications, and use of these devices is expected to grow as the energy sector moves toward hydrogen as an energy carrier. However, an important concern for the usage of PEM fuel cells is their sensitivity to low levels (ppm) of CO. In this respect, various studies have been conducted to explore CO-free fuel processing alternatives [1,2]. A promising method to remove trace amounts of CO from H_2 supplied to the anode is preferential oxidation of CO (PROX) in the presence of excess H_2 [1,3]. An effective PROX catalyst should have high activity for CO oxidation as well as low activity for hydrogen oxidation, typically at low temperatures. For example, a good PROX catalyst should be able to selectively oxidize 10,000 ppm of CO to concentrations of less than 5 ppm, without decreasing the H_2 content of the reformate gas.

The PROX reaction has been studied extensively on supported platinum catalysts such as Pt/Al_2O_3, Pt/A-zeolite, Pt/modernite [4,5]. In recent years, catalytic gold nano particles have attracted attention for PROX applications. Work on supported nano-gold catalysts by Haruta and co-workers [6] has shown that gold, which was considered to be inert for catalytic applications [7], is in fact a good catalyst for low-temperature CO oxidation. Since then, theoretical and experimental studies have been conducted to study CO oxidation on Au [8–16]. Gold in a highly dispersed form also serves as a catalyst for a variety of other chemical reactions [17,18] as well as for the PROX process [19]. Depending on the nature of the support (Al_2O_3, TiO_2, MnO_x, CeO_2 or α-Fe_2O_3) [20–24] and gold particle size, CO and H_2 oxidation reactions are affected to different extents [25]. It has been reported that at low-temperatures Au/α-Fe_2O_3 shows higher PROX selectivity than a commercial Pt/γ-Al_2O_3 catalyst [26]. Therefore, gold-based catalysts at relatively low and stable price compared to platinum group metals, could help reduce the cost of fuel cell technologies [18]. Recent studies have also shown that Cu mixed with ceria oxide is a promising PROX catalyst [27,28]. Other catalytic systems have also been examined for PROX applications, including bimetallic catalysts such as PtSn and PtAu [29,30], and supported Ru, Rh and Pd [31,32] catalysts.

In this study we present results from theoretical calculations to explain the superior low-temperature performance of Au and Cu based catalysts, as compared to more traditional Pt catalysts. We have employed periodic, self-consistent density functional theory (DFT) calculations to address competitive CO oxidation ($CO + O \rightarrow CO_2$) and hydrogen oxidation ($H + O \rightarrow OH$, $H + OH \rightarrow H_2O$, $OH + OH \rightarrow H_2O + O$) on

* To whom correspondence should be addressed.
E-mail: manos@engr.wisc.edu

1011-372X/04/0300–0093/0 © 2004 Plenum Publishing Corporation

Au(111), Cu(111) and Pt(111). The geometry and thermochemistry of various reactive intermediates are presented, as well as reaction pathways and activation energies for these elementary steps. A rigorous barrier analysis scheme is implemented for the appropriate decomposition of the activation energy barrier of each elementary step into three major components. Finally, using the DFT-derived parameters for surface reaction steps and handbook values of gas phase reaction thermochemistry, we construct a simple micro-kinetic model to predict trends in PROX selectivity on Au, Cu and Pt surfaces as a function of temperature.

2. Methods

Self-consistent, periodic, total energy calculations [33] based on gradient-corrected DFT are performed using DACAPO [34]. The Au(111), Cu(111) and Pt(111) surfaces are represented by three-layer slabs, periodically repeated in super cell geometry with four equivalent layers of vacuum between successive metal slabs. A 2×2 unit cell, corresponding to a surface coverage of 0.25 ML, is employed for adsorption studies on each metal. Adsorption is allowed on only one of the two surfaces exposed, and the electrostatic potential is adjusted accordingly [35]. Previous calculations have shown that surface relaxation has only small effects for similar systems [36–40]. Therefore, all the metal atoms are kept fixed at their bulk truncated positions. Ultrasoft Vanderbilt pseudopotentials [41] are employed to describe core electron interactions and the Kohn–Sham one-electron valence states are expanded in a basis of plane waves with kinetic energy upto 25 Ry. The surface Brillouin zone is sampled at 18 special **k** points. Convergence (upto ± 0.1 eV) with respect to the **k** point set as well as with respect to the number of included metal layers is confirmed. The self-consistent PW91 generalized gradient approximation (GGA-PW91) [42,43] is used for describing the exchange-correlation energy and potential. The self-consistent PW91 density is determined by iterative diagonalization of the Kohn–Sham Hamiltonian, Fermi population of the Kohn–Sham states ($k_bT = 0.1$ eV), and Pulay mixing of the resulting electron density [44]. All total energies have been extrapolated to $k_bT = 0$ eV. Zero-point energy corrections are small and not included. The calculated lattice constant is 4.00 Å (experimental value: 3.91 Å) for Pt, 3.66 Å (experimental: 3.61 Å) for Cu and 4.18 Å (experimental: 4.07 Å) for Au [45]. These values are in good agreement with previously published results [38–40, 46–48]. Although all high symmetry sites have been tested for all adsorbates on all three surfaces, only the strongest binding sites are reported here.

Activation energy barriers for the oxidation of carbon monoxide and hydrogen and dissociation of H_2 and O_2 on these surfaces are calculated using the climbing image nudged elastic band (cNEB) method [49,50]. Linear interpolation between the reactant and product states of each elementary step (a total of seven images) are used as initial guesses for the reaction co-ordinate, and the individual images are then optimized with the cNEB algorithm (a constrained molecular dynamics algorithm). For a better resolution of the resulting minimum energy path in the vicinity of the transition state, the image next to the transition state is allowed to ascend the potential energy surface (PES) and reach the saddle point. This image with the highest energy represents the transition state, which is verified by subsequent vibrational modes calculations, yielding only one imaginary frequency [51].

The following barrier decomposition scheme is used to analyze the ($A + B \rightarrow AB$) reaction barriers for a co-adsorbed system of reactants A and B, such as the transition state (TS). E_A^{TS} (E_B^{TS}) is the energy cost for reactant A (B) to move from its position in the initial state to its position at the transition state in the absence of B (A). E_{A+B}^{TS} is the activation energy barrier as calculated by cNEB. E_{int}^{TS}, calculated as $E_{int}^{TS} = E_{A+B}^{TS} - (E_A^{TS} + E_B^{TS})$, is a measure of the interaction between A and B at the transition state. A negative E_{int}^{TS} value implies attraction whereas a positive E_{int}^{TS} value implies repulsion between A and B at the transition state.

Micro-kinetic modeling [52] using the DFT-derived parameters for surface reaction steps and handbook values for gas phase reaction thermochemistry [53], is carried out using ATHENA Visual Workbench [54].

3. Results and discussion

3.1. Atomic and molecular adsorption on Au(111), Cu(111) and Pt(111)

A summary of the preferred adsorption states and the corresponding binding energies on Au(111), Cu(111) and Pt(111) is given in table 1. In general, atomic adsorbates, hydrogen (H) and oxygen (O), prefer the fcc site on each of these metals and they bind the weakest on Au(111). Adsorption of H atoms has a very flat PES on Pt(111). On all three surfaces, carbon monoxide binds perpendicular to the surface through its C end and hydroxyl species binds through the O end, either perpendicular or in a tilted configuration. On Au(111), CO binds weakly and has a relatively flat PES. The binding energy for CO adsorption is significantly higher on Pt(111) as compared to Au(111) and Cu(111). The geometry of water changes little upon adsorption, with the two O—H bonds lying in a plane parallel to the metal surface (referred to as "top flat" in the table) [55]. Carbon dioxide interacts very weakly with these surfaces (binding energy ca −0.1 eV) and its optimized geometry resembles a linear gas phase molecule, parallel and quite far from the surface.

Table 1
Summary of the preferred adsorption sites, and the co-adsorption sites corresponding to the minimum energy path, and binding energy in (eV) for various adsorbates on Au(111), Cu(111) and Pt(111)

Species	Au(111)		Cu(111)		Pt(111)	
O	fcc	−2.71	fcc	−4.41	fcc	−3.73
H	fcc	−2.25	fcc	−2.55	fcc/top	−2.71
CO	fcc perpendicular	−0.40	fcc perpendicular	−0.96	fcc perpendicular	−1.81
OH	bridge tilted	−1.74	fcc perpendicular	−2.85	top tilted	−2.09
H_2O	top flat	−0.17	top flat	−0.18	top flat	−0.27
CO_2	Linear (similar to gas phase), and parallel at C-M > 3.6 Å, binds with BE ca −0.1 eV					
CO + O	CO: top O: fcc	−3.25	CO: top O: fcc	−5.20	CO: top O: fcc	−5.33
O + H	O: fcc H: fcc	−4.61	O: fcc H: fcc	−6.38	O: fcc H: top	−6.44
OH + OH	OH: top tilted OH: bridge tilted	−3.65	both on bridge tilted	−5.71	OH: top tilted OH: bridge tilted	−4.56
H_2O + O	H_2O: top flat O: fcc	−3.17	H_2O: top flat O: fcc	−5.19	H_2O: top flat O: fcc	−4.10

Note: Binding Energy (BE) = $E_{\text{slab + adsorbate}} - E_{\text{clean slab}} - E_{\text{adsorbate (g)}}$. Results correspond to a (2 × 2) unit cell.

3.2. Thermochemistry of co-adsorption and of CO and H oxidation

One-dimensional PES showing the thermochemistry and activation energy barriers for CO oxidation and H oxidation on Au(111), Cu(111) and Pt(111) are presented in figure 1a, b and c, respectively. The PES is constructed by taking gas phase atomic oxygen, adsorbed atomic hydrogen and adsorbed carbon monoxide as the reference state (zero of the energy axis). Insets in figure 1 shows the geometries of the initial, transition and final states for the elementary steps on each surface. The energy change for each step is tabulated in table 2. Both CO oxidation and OH formation are exothermic on these surfaces, on Au being the most exothermic, and on Pt being the least exothermic. These figures also give insight into the amount of stabilization or destabilization that occurs upon co-adsorption (ca) (total coverage of 0.50 ML) in comparison to the state where the adsorbates are adsorbed individually in the unit cell (inf) (0.25 ML). The amount of stabilization can be calculated from table 1 where the thermochemistry and the geometry of the co-adsorbed state are given. As shown in figure 1a, b and c, there is an attractive stabilization between H_2O and O when co-adsorbed on all three surfaces. There is also a stabilization on Au(111) and Pt(111) when two OH species are co-adsorbed, whereas there is minimal interaction in the corresponding case on Cu(111). In contrast, we find repulsion between co-adsorbed O and H on Au(111) and Cu(111), while there is no interaction between these species on Pt(111). Co-adsorption of CO and O on Pt(111) and Cu(111) leads to repulsion, whereas there is attraction between these species on Au(111).

3.3. Reaction path for CO and H oxidation

3.3.1. CO oxidation ($CO + O \rightarrow CO_2$)

As shown in table 1 and figure 1a, b and c, when co-adsorbed, CO prefers the top site and O prefers the fcc site on all investigated surfaces. At the transition state, CO is tilted slightly on the top site whereas O has moved from the fcc site to the bridge site. The activation energy barriers for this step on Au(111), Cu(111) and Pt(111) are 0.18, 0.82 and 0.96 eV, respectively. These values are in good agreement with the activation energy barriers for CO oxidation reported in the literature [22,56,57]. As shown in figure 2, analysis of the CO + O reaction barrier using the barrier decomposition scheme described earlier, indicates that the activation of atomic oxygen contributes the major portion of the overall activation barrier; there is only a small amount of interaction ($|E_{\text{int}}^{\text{TS}}| < 0.10$ eV) between CO and O at the transition state.

3.3.2. Partial H oxidation ($H + O \rightarrow OH$)

The reaction pathway for OH formation is similar on Au(111) and Cu(111), as shown in figure 1a and b. Adsorbed O and H experience repulsion when they are co-adsorbed, and both atoms prefer fcc sites in the co-adsorbed state. At the transition state on these surfaces, H has moved from the fcc site towards the bridge site, while O remains near the fcc site. The final state of this elementary step involves an OH adsorbed tilted on a bridge site on Au(111) or a fcc site on Cu(111). On Pt(111), however, the pathway is different. As shown in figure 1c, to reach the transition state, H moves from the top site to the off-top position approaching the O that has moved from the fcc to the bridge site. After the OH bond is formed, OH moves to its preferred top-tilted configuration. The values of the activation barrier for this step are 0.90, 1.28 and 0.83 eV on Au(111), Cu(111) and Pt(111), respectively. The value of the activation barrier on Pt(111) agrees well with the DFT value of 0.87 eV reported by Michaelides and Hu [36]. Barrier decomposition analysis for the oxidation of H by O, as shown in figure 2, indicates that unlike the CO oxidation reaction, this barrier has significant contributions from the activation of both O

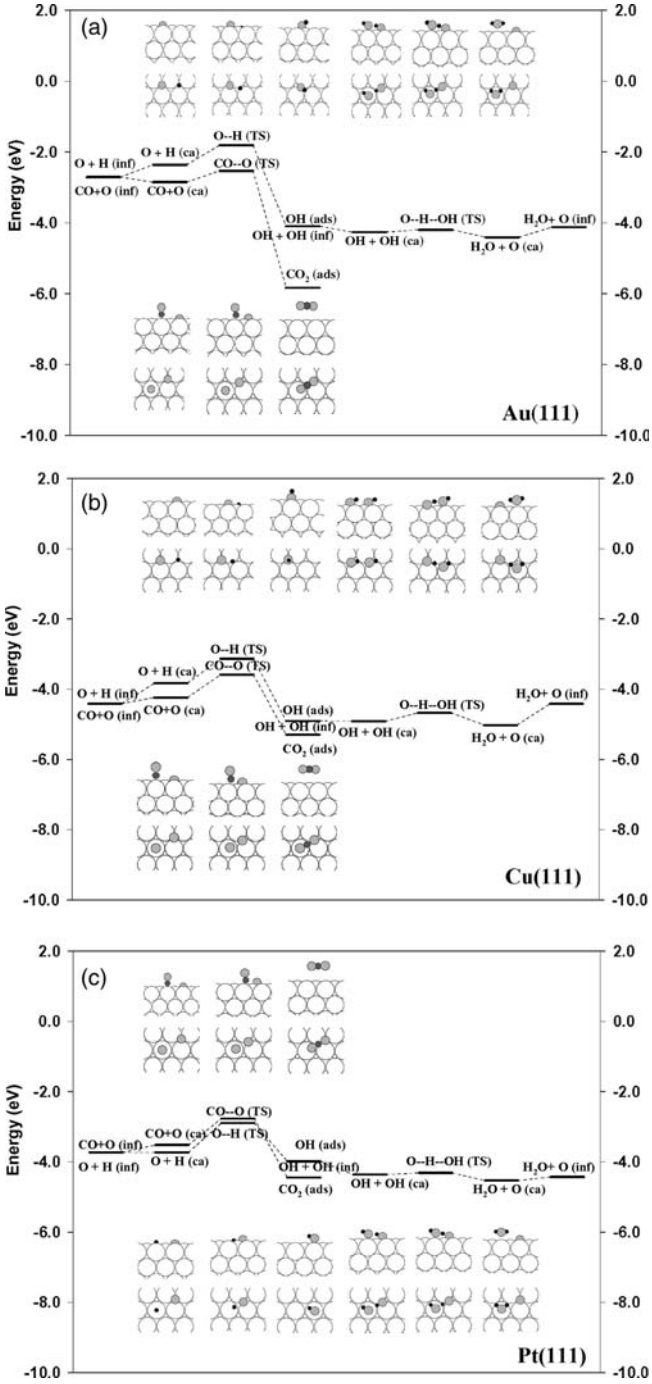

Figure 1. PES showing the thermochemistry and activation energy barriers of the competitive CO and H oxidation on Au(111) (a), Cu(111) (b) and Pt(111) (c). Atomic oxygen in the gas phase, with atomic hydrogen and carbon monoxide adsorbed on the surface, has been taken as the reference state (zero of the energy axis). ''ca'' corresponds to the co-adsorbed state (total coverage of 0.50 ML) and ''inf'' refers to the state when the adsorbates are adsorbed in separate unit cells (coverage of 0.25 ML). The stabilization/destabilization upon co-adsorption is reflected in the energy difference between the ''inf'' and ''ca'' states. The geometry (top and cross-section views) of the initial state (ca), transition state (TS) and the final state (ads or ca) are shown in the snapshots inserted in each figure. For simplicity OH (ads) and OH + OH (inf) have been put at the same energy level. Although not shown here, O_2 and H_2 dissociation on all three metals has been accounted for in the micro-kinetic model (see text and table 2).

and H. Also at the transition state, O and H experience significant repulsion on all the three surfaces, which contributes a further increase to the overall OH formation barrier.

3.3.3. *Complete H oxidation to H_2O*

Formation of H_2O can take place either by H addition to OH ($H + OH \rightarrow H_2O$) or by OH-disproportionation ($OH + OH \rightarrow H_2O + O$). As reported

Table 2
Thermochemistry and activation energy barriers of the competitive surface reactions for PROX

Elementary step	Heat of reaction ΔH_s (eV) infinite separation (co-adsorbed)			Activation energy barrier (eV) infinite separation (co-adsorbed)		
	Au (111)	Cu (111)	Pt (111)	Au (111)	Cu (111)	Pt (111)
$CO + O \rightarrow CO_2$	−3.12(−2.98)	−0.87(−1.04)	−0.72(−0.93)	0.18(0.32)	0.82(0.65)	0.96(0.75)
$O + H \rightarrow OH$	−1.38(−1.73)	−0.48(−1.06)	−0.26(−0.26)	0.90(0.55)	1.28(0.70)	0.83(0.83)
$OH + OH \rightarrow H_2O + O$	−0.03(−0.15)	0.49(−0.10)	−0.44(−0.16)	–(0.07)	0.23(0.24)	–(0.05)
$OH + H \rightarrow H_2O$	−1.40(−1.59)	0.01(−0.35)	−0.70(−0.74)	0.55(0.36)	1.35(0.99)	0.18(0.14)
H_2 (g) $\rightarrow H + H$[b]	0.13(0.43)	−0.30(−0.26)	−0.79(−0.70)	1.13	0.70	0.00
$O_2 \rightarrow O + O$[c]	0.16(0.58)	−2.37(−0.54)	−1.50(−0.93)	0.95	0.20	0.77

Note: ΔH_g is the heat of reaction occurring in the gas phase[a] (negative for exothermic). ΔH_s is the heat of reaction occurring on the surface and is calculated as $\Delta H_s = -\Sigma BE_{reactants} + \Sigma BE_{products} + \Delta H_g$. Infinite separation refers to the adsorbates adsorbed individually in the (2 × 2) unit cell whereas co-adsorbed refers to the adsorbates adsorbed together in the unit cell. '–' denotes that the infinite separation numbers for the activation energy barriers are irrelevant as the transition state is more stable than the infinite separation state of OH + OH which is due to a large stabilization of the co-adsorbed OH + OH state.

[a]The gas phase bond energies (ΔH_g) from DFT are:
$CO + O \rightarrow CO_2$ ($\Delta H_g = -6.17$ eV); $O + H \rightarrow OH$ ($\Delta H_g = -4.61$ eV)
$OH + OH \rightarrow H_2O + O$ ($\Delta H_g = -0.63$ eV); $OH + H \rightarrow H_2O$ ($\Delta H_g = -5.23$ eV)
$H_2 \rightarrow H + H$ ($\Delta H_g = 4.57$ eV); $O_2 \rightarrow O + O$ ($\Delta H_g = 5.64$ eV).

[b] See Ref. [Greeley and Mavrikakis, in preparation].

[c] See Ref. [38, 39, Xu *et al.*, Submitted for publication] – Note that the values for O_2 dissociation on Au correspond to the (211) surface.

in table 2, the disproportionation reaction is the kinetically preferred route on all three surfaces. On Cu(111), the two co-adsorbed OH species prefer the adjacent bridge tilted sites. At the transition state, one of the OH species has moved towards the top site and the other one begins to share its H atom while moving towards the fcc site. As shown in figure 1b, in the final state, the H_2O molecule lies parallel to the surface whereas the O atom occupies an fcc site. This reaction step has an activation barrier of 0.24 eV. For OH-disproportionation on Au(111) and Pt(111), the stable co-adsorbed state has one OH in the top tilted and the other OH in the bridge tilted state. At the transition state, the OH at the top site takes the H from the OH at the bridge tilted site, which is on its way to the adjacent fcc site, forming a final state similar to that on Cu(111) (see figure 1a and c). The values of the activation energy barrier for this step on both Au(111) and Pt(111) are low (< 0.10 eV),

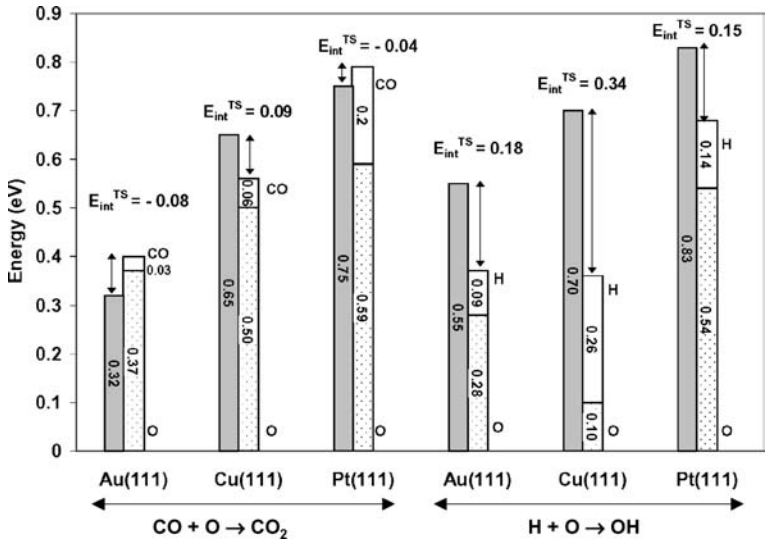

Figure 2. Barrier decomposition analysis of the CO + O and O + H reactions on Au(111), Cu(111) and Pt(111). ▨ represents E^{TS}_{A+B}, which is the calculated overall activation energy barrier (co-adsorbed), as reported in table 2. ▩ represents the energy cost E^{TS}_{A} for atomic oxygen activation, whereas □ represents the energy cost E^{TS}_{b} for carbon monoxide (in case of CO + O) or atomic hydrogen (in the case of O + H) activation. Negative values of E^{TS}_{int} indicate attraction and positive values indicate repulsion at the transition state.

implying an almost spontaneous elementary reaction step.

3.4. Comparison of the kinetics of CO and H oxidation on Au(111), Cu(111) and Pt(111)

A summary of the thermochemistry and activation energy barriers for the oxidation reactions of adsorbed CO and H on Au, Cu and Pt is presented in table 2. On all three surfaces studied, the formation of OH ($O + H \rightarrow OH$) has a higher activation energy barrier than the step yielding H_2O ($OH + OH \rightarrow H_2O + O$). This result, in combination with the similar barriers for $OH + OH \rightarrow H_2O + O$ on all three surfaces, suggests that selectivity for PROX catalysts is mainly determined by the relative CO_2 and OH formation rates, at least for the specific reaction mechanisms considered here. As briefly discussed in the subsequent sections of this paper, other mechanisms might contribute to PROX, and one cannot exclude the possibility that other steps, associated with these alternative reaction mechanisms, might determine selectivity.

The barrier for CO oxidation on Au(111) is only 0.18 eV, which is much lower than the barrier for OH formation (0.90 eV). On Cu(111), the barrier for CO oxidation is 0.82 eV, which is again lower than the OH formation barrier (1.28 eV). In contrast, on Pt(111) the barrier for OH formation (0.83 eV) is lower than for CO oxidation (0.96 eV). These results explain why Au and Cu catalysts are both more selective catalysts than Pt for the preferential oxidation of CO in the presence of excess hydrogen at low temperatures. A more refined analysis of this argument is provided subsequently via a micro-kinetic model for PROX.

3.5. Micro-kinetic model for PROX

Although defects and lower symmetry sites may dominate catalytic rates [58–60], we used parameters determined on (111) surfaces for elucidating basic *trends* in PROX selectivity, with the exception of O_2 dissociation on Au, one of the most activated steps, where we used the calculated barrier on the (211) surface. Nevertheless, since O_2 dissociation is a *common* step for both CO and H oxidation, the specific value of this barrier should not affect reaction selectivity. In the micro-kinetic model, we used the barrier to H_2 dissociation on Au(111), but our selectivity trend results did not change upon decreasing that barrier to zero, suggesting that even if we would have considered H_2 dissociation on Au(211), our conclusions regarding selectivity would not have changed. Furthermore, for the case of Au, where CO and hydrogen oxidation may proceed via alternative paths, possibly involving molecular oxygen [10], we have considered only the routes proceeding via atomic oxygen for the purposes of this study. The elementary steps included in the PROX micro-kinetic model are as follows, where * refers to a catalytic site.

$$CO(g) + * \rightarrow CO* \quad (1)$$

$$H_2(g) + 2* \rightarrow 2H* \quad (2)$$

$$O_2(g) + 2* \rightarrow O_2** \quad (3)$$

$$O_2** \rightarrow 2O* \quad (4)$$

$$O* + H* \rightarrow OH* + * \quad (5)$$

$$OH* + H* \rightarrow H_2O* + * \quad (6)$$

$$OH* + OH* \rightarrow H_2O* + O* \quad (7)$$

$$CO* + O* \rightarrow CO_2* + * \quad (8)$$

$$H_2O* \rightarrow H_2O(g) + * \quad (9)$$

$$CO_2* \rightarrow CO_2(g) + * \quad (10)$$

Values for the rate constants in the micro-kinetic model are derived from the DFT results reported in tables 1 and 2. For the activation energy barriers, we used the infinite separation activation energy barriers as tabulated in table 2. In addition, dissociation of O_2 (Step 4) is activated on all three metals [38,39,48, Xu *et al.*, Submitted for publication], whereas the dissociative adsorption of H_2 (Step 2) is spontaneous on Pt(111) and activated on Au(111) and Cu(111) [Greeley and Mavrikakis, in preparation]. The activation energy barriers for H_2 and O_2 dissociation on all three metals are given in table 2. Our model assumes that the values of the kinetic parameters for the oxidation of CO and H are not affected by the presence of H and CO, respectively. Furthermore, for Cu(111) and Au(111), characterized by low sticking probabilities of O_2 and therefore low oxygen coverage, we assume that if the kinetics of the two competing oxidation reactions change, they will do so in a similar way, so that reaction selectivity on these surfaces remains invariant with respect to coverage. The micro-kinetic simulations are run under the reaction conditions of PROX experiments conducted by Avgouropoulos *et al.* [26] (reaction mixture consisting of 1 vol% CO, 1.25% O_2 and 50 vol% H_2 at a pressure of 1 atm). The calculated selectivities of the three catalysts at two representative temperatures (423 and 823 K) are shown in table 3. We note here that this temperature range is substantially higher than the experimentally determined temperature range of interest with respect to PROX reactivity. This difference is most likely related to the fact that we consider activity on the (111) surfaces for the purpose of this study. The discrepancy in temperature range would likely be minimized if the elementary steps were studied on a model stepped surface (e.g. (211)). Nevertheless, we suggest that our results provide useful insights regarding an initial comparison between PROX selectivities on the three metals.

Table 3
Results from the PROX micro-kinetic model

	Au(111)		Cu(111)		Pt(111)	
Temperature (K)	423	823	423	823	423	823
Selectivity (%)	100.00	6.88	100.00	96.95	32.98	18.71
$k_{f,8}/k_{f,5}$	3.77×10^{8}	2.56×10^{4}	3.01×10^{5}	6.56×10^{2}	2.83×10^{-2}	1.60×10^{-1}
Θ_{CO}/Θ_{H}	1.17×10^{-3}	2.66×10^{-6}	4.49	0.02	17.40	1.44
$(k_{f,8}/k_{f,5}) \times (\Theta_{CO}/\Theta_{H})$	4.41×10^{5}	6.82×10^{-2}	1.35×10^{6}	1.59×10^{1}	0.49	0.23

Note: Selectivity is defined as Selectivity (%) = 0.5* ($[CO]_{in} - [CO]_{out}$)/($[O_2]_{in} - [O_2]_{out}$)* 100. The ratio of the coverage of adsorbed CO and H on the metal surface is represented by Θ_{CO}/Θ_{H}. $k_{f,8}$ is the forward rate constant for Step 8 (CO* + O* $\rightarrow$ CO_2* + *). $k_{f,5}$ is the forward rate constant for Step 5 (O* + H* $\rightarrow$ OH* + *). Rate constant is defined as $Ae^{-E/RT}$ where A is the pre-exponential factor (assumed identical for steps 5 and 8), E is the activation energy barrier, R is the ideal gas constant and T is the temperature. For comments related to the temperature range listed here, see discussion in the micro-kinetic model section of the text.

At low-temperatures (423 K) as indicated in table 3, the selectivity for CO oxidation on Au and Cu catalysts is ~100%, whereas Pt shows a significantly lower selectivity (~33%). At higher temperatures (823 K), Cu and Pt catalysts lose some selectivity while Au loses a substantial fraction of its selectivity.

The selectivity for PROX catalysts is dependent on the relative rates of Steps 8 and 5. As shown in table 3, at low temperature the ratio $k_{f,8}/k_{f,5}$ is significantly higher for Au and Cu compared to Pt. As temperature increases, the $k_{f,8}/k_{f,5}$ ratio decreases for Au and Cu but increases for Pt. The other factor contributing to the relative rates of Steps 8 and 5 is the relative coverages of CO and H adsorbed on these surfaces. The coverage of H reflects the balance between the dissociative H_2 adsorption and the steps leading to H_2O formation. Similarly, the CO coverage reflects the balance between CO adsorption and its oxidation. Schubert *et al.* have also implicated the steady state coverage by CO in explaining the dependence of CO selectivity on temperature for Au versus Pt catalysts [61]. They have observed that the coverage of CO on platinum is usually near saturation under reaction conditions, whereas the coverage of CO on Au depends on the partial pressure of CO. table 3 shows that the ratio of surface coverages, Θ_{CO}/Θ_{H} is highest on Pt(111) (> Cu(111) > Au(111)) at both temperatures. The ratio Θ_{CO}/Θ_{H} decreases as temperature increases, and this decrease is much more significant on Au than on Cu.

As shown in table 3, incorporating the effects of rate constants and surface coverages through the ratio $(k_{f,8}/k_{f,5}) \times (\Theta_{CO}/\Theta_{H})$ explains the experimentally observed selectivity trends. The high selectivity of Cu and Au catalysts at low-temperatures is due to high values of $k_{f,8}/k_{f,5}$. As temperature increases, Pt shows a small loss in selectivity, since the decrease in Θ_{CO}/Θ_{H} is compensated by an increase in $k_{f,8}/k_{f,5}$. The selectivity of Au decreases at higher temperatures, because the values of Θ_{CO}/Θ_{H} as well as $k_{f,8}/k_{f,5}$ both decrease. This behavior also applies to Cu, but the decreases in Θ_{CO}/Θ_{H} and $k_{f,8}/k_{f,5}$ with temperature are less significant than for Au.

The results of this study provide a theoretical framework for the interpretation of recent experimental findings which show that catalysts based on Au and Cu based catalysts are superior to Pt-based catalysts for the oxidation of trace CO in reformate gases at low temperatures. Pursuing this CO removal at temperatures close to operational temperatures for low-temperature fuel cells is clearly beneficial.

4. Conclusions

Periodic, self-consistent, DFT calculations have been used to study the selective oxidation of CO with respect to H_2 on Au(111), Pt(111) and Cu(111). On all these surfaces, and for the specific reaction mechanism considered, the OH formation step competes with the CO oxidation step. The relative rates of these two steps appear to determine PROX selectivity. The results of our calculations give a barrier of 0.18 eV for CO oxidation versus a barrier of 0.90 eV for OH formation on Au(111). Similarly, Cu(111) shows a lower barrier for CO oxidation (0.82 eV) than H oxidation (1.28 eV), whereas Pt(111) shows a higher barrier for CO oxidation (0.96 eV) than H oxidation (0.83 eV). A micro-kinetic model based on DFT derived parameters suggests that PROX selectivity is determined both by the kinetics of the competing CO and H oxidation reactions and by the coverages of CO and H on the metal surfaces. We have shown that at low-temperatures both Au and Cu should be more selective PROX catalysts than Pt. At higher temperatures, Pt and Cu lose a small fraction of their selectivity, whereas Au shows a substantial selectivity loss, mainly because of the weak CO binding.

Acknowledgment

We used computational resources at the National Energy Research Scientific Computing Center (NERSC), which is supported by the Office of Science of the US Department of Energy under Contract No. DE-AC03-76SF00098. The authors acknowledge partial

support from NSF cooperative agreement ACI-9619020 through computing resources provided by the National Partnership for Advanced Computing Infrastructure (NPACI). MM acknowledges partial financial support from an NSF-CAREER Award (CTS-0134561) and a 3M-faculty award. This work was partially supported by a US Department of Energy, Office of Basic Energy Sciences, through a Catalysis Science Grant DE-FG02-03ER15469. LCG thanks DAAD for a US-German exchange fellowship. We thank Prof. Warren Stewart for fruitful discussions on using Athena for micro kinetic modeling, and Jeff Greeley and Ye Xu for sharing their results on H_2 and O_2 dissociation on the three surfaces studied.

References

[1] T.V. Choudhary and D.W. Goodman, Catal. Today 77 (2002) 65.
[2] R.R. Davda and J.A. Dumesic, Angew. Chem. Int. Ed. 42 (2003) 4068.
[3] O. Korotkikh and R. Farrauto, Catal. Today 62 (2000) 249.
[4] H. Igarashi, H. Uchida, M. Suzuki, Y. Sasaki and M. Watanabe, Appl. Catal. A Gen. 159 (1997) 159.
[5] M.J. Kahlich, H.A. Gasteiger and R.J. Behm, J. Catal. 171 (1997) 93.
[6] M. Haruta, S. Tsubota, T. Kobayashi, H. Kageyama, M.J. Genet and B. Delmon, J. Catal. 144 (1993) 175.
[7] B. Hammer and J.K. Nørskov, Nature 376 (1995) 238.
[8] M. Mavrikakis, P. Stoltze and J.K. Nørskov, Catal. Lett. 64 (2000) 101.
[9] Z.P. Liu, P. Hu and A. Alavi, J. Am. Chem. Soc. 124 (2002) 14770.
[10] N. Lopez and J.K. Nørskov, J. Am. Chem. Soc. 124 (2002) 11262.
[11] V.A. Bondzie, S.C. Parker and C.T. Campbell, Catal. Lett. 63 (1999) 143.
[12] C.K. Costello, M.C. Kung, H.S. Oh, Y. Wang and H.H. Kung, Appl. Catal. A Gen. 232 (2002) 159.
[13] H.H. Kung, M.C. Kung and C.K. Costello, J. Catal. 216 (2003) 425.
[14] L.M. Molina and B. Hammer, Phys. Rev. Lett. 90 (2003).
[15] M. Valden, X. Lai and D.W. Goodman, Science 281 (1998) 1647.
[16] F. Boccuzzi, A. Chiorino, S. Tsubota and M. Haruta, J. Phys. Chem.-Us 100 (1996) 3625.
[17] A. Cho, Science 299 (2003) 1684.
[18] D. Cameron, R. Holliday and D. Thompson, J. Power Sources 118 (2003) 298.
[19] T.V. Choudhary and D.W. Goodman, Top. Catal. 21 (2002) 25.
[20] R.M.T. Sanchez, A. Ueda, K. Tanaka and M. Haruta, J. Catal. 168 (1997) 125.
[21] R.J.H. Griesel and B.E. Nieuwenhuys, J. Catal. 199 (2001) 48.
[22] M.J. Kahlich, H.A. Gasteiger and R.J. Behm, J. Catal. 182 (1999) 430.
[23] G.K. Bethke and H.H. Kung, Appl. Catal. A Gen. 194 (2000) 43.
[24] T.V. Choudhary, C. Sivadinarayana, C. Chusuei, A.K. Datye, J.P. Fackler Jr and D.W. Goodman, J. Catal. 207 (2002) 247.
[25] M.M. Schubert, V. Plzak, J. Garche and R.J. Behm, Catal. Lett. 76 (2001) 143.
[26] G. Avgouropoulos, T. Ioannides, C. Papadopoulou, J. Batista, S. Hocevar and H.K. Matralis, Catal. Today 75 (2002) 157.
[27] G. Avgouropoulos, T. Ioannides, H.K. Matralis, J. Batista and S. Hocevar, Catal. Lett. 73 (2001) 33.
[28] D.H. Kim and J.E. Chua, Catal. Lett. 86 (2003) 107.
[29] M.M. Schubert, M.J. Kahlich, G. Feldmeyer, M. Huttner, S. Hackenberg, H.A. Gasteiger and R.J. Behm, Phys. Chem. Chem. Phys. 3 (2001) 1123.
[30] J. Zhang, Y. Wang, B. Chen, C. Li, D. Wu and X. Wang, Energy Conv. Mgmt. 44 (2003) 1805.
[31] P.V. Snytnikov, V.A. Sobyanin, V.D. Belyaev, P.G. Tsyrulnikov, N.B. Shitova and D.A. Shlyapin, Appl. Catal. A Gen. 239 (2003) 149.
[32] H. Tanaka, S. Ito, S. Kameoka, K. Tomishige and K. Kunimori, Catal. Commun. 4 (2003) 1.
[33] J. Greeley, J.K. Nørskov and M. Mavrikakis, Ann. Rev. Phys. Chem. 53 (2002) 319.
[34] B. Hammer, L.B. Hansen and J.K. Nørskov, Phys. Rev. B 59 (1999) 7413.
[35] J. Neugebauer and M. Scheffler, Phys. Rev. B 46 (1992) 16067.
[36] A. Michaelides and P. Hu, J. Am. Chem. Soc. 122 (2000) 9866.
[37] A. Michaelides and P. Hu, J. Am. Chem. Soc. 123 (2001) 4235.
[38] Y. Xu and M. Mavrikakis, Surf. Sci. 494 (2001) 131.
[39] Y. Xu and M. Mavrikakis, J. Phys. Chem. B 107 (2003) 9298.
[40] J. Greeley and M. Mavrikakis, J. Am. Chem. Soc. 124 (2002) 7193.
[41] D. Vanderbilt, Phys. Rev. B 41 (1990) 7892.
[42] J.P. Perdew, J.A. Chevary, S.H. Vosko, K.A. Jackson, M.R. Pederson, D.J. Singh and C. Fiolhais, Phys. Rev. B 46 (1992) 6671.
[43] J.A. White and D.M. Bird, Phys. Rev. B 50 (1994) 4954.
[44] G. Kresse and J. Furthmuller, Comput. Mater. Sci. 6 (1996) 15.
[45] *CRC Handbook of Chemistry and Physics*, 76th edn., ed. D.R. Lide (CRC Press, New York, 1996).
[46] J. Greeley and M. Mavrikakis, J. Catal. 208 (2002) 291.
[47] J. Greeley, A.A. Gokhale, J. Kreuser, J.A. Dumesic, H. Topsoe, N.Y. Topsoe and M. Mavrikakis, J. Catal. 213 (2003) 63.
[48] Y. Xu and M. Mavrikakis, Surf. Sci. 538 (2003) 219.
[49] G. Henkelman, B.P. Uberuaga and H. Jonsson, J. Chem. Phys. 113 (2000) 9901.
[50] G. Henkelman and H. Jonsson, J. Chem. Phys. 113 (2000) 9978.
[51] J. Greeley and M. Mavrikakis, Surf. Sci. 540 (2003) 215.
[52] J.A. Dumesic, *The Microkinetics of Heterogeneous Catalysis*. ACS professional reference book. Vol. XII (American Chemical Society, Washington, DC, 1993).
[53] P.J. Linstrom and W.G. Mallard, eds. *NIST Chemistry WebBook, NIST Standard Reference Database Number 69* (National Institute of Standards and Technology, Gaithersburg MD, 2003) (http://webbook.nist.gov).
[54] W.E. Stewart, M. Caracotsios and J.P. Sorensen, AIChE J. 38 (1992) 641.
[55] A. Michaelides, V.A. Ranea, P.L. de Andres and D.A. King, Phys. Rev. Lett. 90 (2003) 216102.
[56] A. Eichler, Surf. Sci. 498 (2002) 314.
[57] C.J. Zhang, R.J. Baxter, P. Hu, A. Alavi and M.H. Lee, J. Chem. Phys. 115 (2001) 5272.
[58] M. Mavrikakis, M. Bäumer, H.J. Freund and J.K. Nørskov, Catal. Lett. 81 (2002) 153.
[59] S. Dahl, A. Logadottir, R.C. Egeberg, J.H. Larsen, I. Chorkendorff, E. Tornqvist and J.K. Nørskov, Phys. Rev. Lett. 83 (1999) 1814.
[60] J.K. Nørskov, *et al.*, J. Catal. 209 (2002) 275.
[61] M.M. Schubert, M.J. Kahlich, H.A. Gasteiger and R.J. Behm, J. Power Sources 84 (1999) 175.